PROCEEDINGS OF SPIE

SPIEDigitalLibrary.org/conference-proceedings-of-spie

Characterization and calibration of the James Webb space telescope mirror actuators fine stage motion

Taylor S. Chonis, Ben B. Gallagher, J. Scott Knight, D. Scott Acton, Koby Z. Smith, et al.

Taylor S. Chonis, Ben B. Gallagher, J. Scott Knight, D. Scott Acton, Koby Z. Smith, Erin Wolf, Eric Coppock, James Tersigni, Thomas Comeau, "Characterization and calibration of the James Webb space telescope mirror actuators fine stage motion," Proc. SPIE 10698, Space Telescopes and Instrumentation 2018: Optical, Infrared, and Millimeter Wave, 106983S (12 July 2018); doi: 10.1117/12.2311815

SPIE.

Event: SPIE Astronomical Telescopes + Instrumentation, 2018, Austin, Texas, United States

Characterization and calibration of the James Webb Space Telescope mirror actuators fine stage motion

Taylor S. Chonis*[a], Ben B. Gallagher[b], J. Scott Knight[a], D. Scott Acton[a], Koby Z. Smith[a], Erin Wolf[a], Eric Coppock[a], James Tersigni[a], Thomas Comeau[c]

[a]Ball Aerospace, 1600 Commerce Street, Boulder, CO, USA 80301
[b]Thirty Meter Telescope, 100 West Walnut Street, Suite 300, Pasadena, CA, USA 91124
[c]Space Telescope Science Institute, 3700 San Martin Drive, Baltimore, MD USA 21218

ABSTRACT

The James Webb Space Telescope's (Webb's) deployable primary and secondary mirrors are actively controlled to achieve and maintain precise optical alignment on-orbit. Each of the 18 primary mirror segment assemblies (PMSAs) and the secondary mirror assembly (SMA) are controlled in six degrees of freedom by using six linear actuators in a hexapod arrangement. In addition, each PMSA contains a seventh actuator that adjusts radius of curvature (RoC). The actuators are of a novel stepper motor-based cryogenic two-stage design that is capable of sub-10 nm motion accuracy over a 20 mm range. The nm-level motion of the 132 actuators were carefully tested and characterized before integration into the mirror assemblies. Using these test results as an initial condition, knowledge of each actuator's length (and therefore mirror position) has relied on software bookkeeping and configuration control to keep an accurate motor step count from which actuator position can be calculated. These operations have been carefully performed through years of Webb test operations using both ground support actuator control software as well as the flight Mirror Control Software (MCS). While the actuator's coarse stage length is cross-checked using a linear variable differential transformer (LVDT), no on-board cross-check exists for the nm-level length changes of the actuators' fine stage. To ensure that the software bookkeeping of motor step count is still accurate after years of testing and to test that the actuator position knowledge was properly handed off from the ground software to the flight MCS, a series of optical tests were devised and performed through the Center of Curvature (CoC) ambient optical test campaigns at the Goddard Space Flight Center (GSFC) and during the thermal-vacuum tests of the entire optical payload that were conducted in Chamber A at Johnson Space Center (JSC). In each test, the actuator Fine Step Count (FSC) value is compared to an external measurement provided by an optical metrology tool with the goal of either confirming the MCS database value, or providing a recommendation for an updated calibration if the measured FSC differs significantly from the MCS-based expectation. During ambient testing of the PMSA hexapods, the nm-level actuator length changes were measured with a custom laser deflectometer by measuring tilts of the PMSA. The PMSA RoC fine stage characterization was performed at JSC using multi-wave interferometric measurements with the CoC Optical Assembly (COCOA). Finally, the SMA hexapod fine stage characterization test was performed at JSC using the NIRCam instrument in the "pass-and-a-half" test configuration using a test source from the Aft-Optics System Source Plate Assembly (ASPA). In this paper, each of these three tests, subsequent data analyses, and uncertainty estimations will be presented. Additionally, a summary of the ensemble state of Webb's actuator fine stages is provided, along with a comparison to a Wavefront Sensing & Control (WFSC)-based requirement for FSC errors as they relate to the optical alignment convergence of the telescope on-orbit.

Keywords: James Webb Space Telescope, segmented mirror, mirror actuators, hexapod, radius of curvature, metrology, interferometry, deflectometry

1. INTRODUCTION

The James Webb Space Telescope[1] (Webb) is a deployable, 6.5 m infrared astronomical observatory that will operate at cryogenic temperatures in an orbit about the second Lagrange point. Because of the large, corrected field of view that is needed to meet Webb's science mission requirements, the Optical Telescope Element (OTE) optical design is a three-

* tchonis@ball.com; phone 1-303-939-4191; http://www.ball.com/aerospace

Space Telescopes and Instrumentation 2018: Optical, Infrared, and Millimeter Wave, edited by Makenzie Lystrup, Howard A. MacEwen, Giovanni G. Fazio, Proc. of SPIE Vol. 10698, 106983S
 · doi: 10.1117/12.2311815

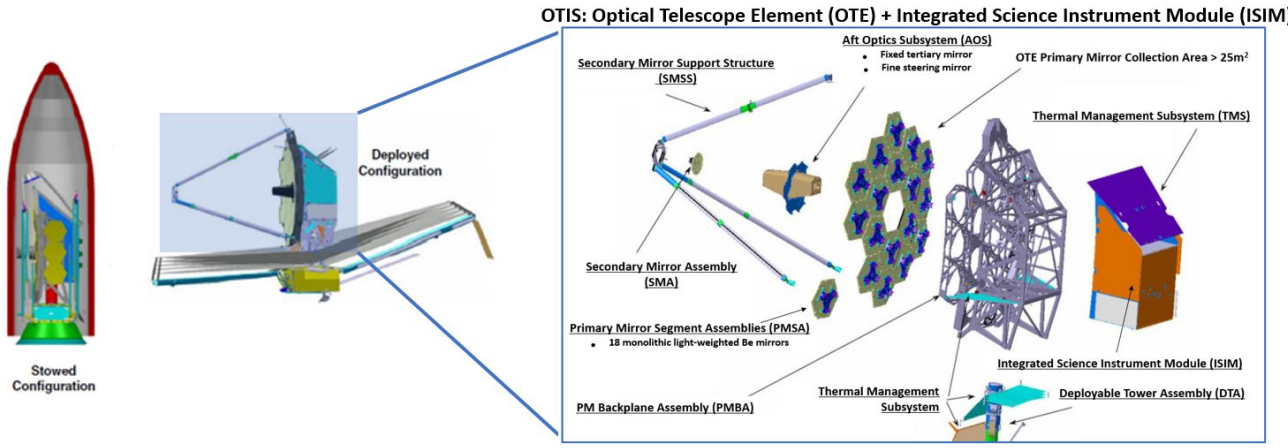

Figure 1. Overview of the Webb observatory. A view of the observatory in the stowed configuration within the Ariane 5 fairing is shown at left. In the center, the observatory can be seen in its deployed configuration. At right is an exploded view of the OTIS with the various subsystems and components within the OTE identified.

mirror anastigmat, which consists of a parabolic primary mirror (PM), a convex hyperbolic secondary mirror (SM), and a concave elliptical tertiary mirror (TM). A flat fine steering mirror (FSM) is also incorporated into the design to fold the optical system and provide image stabilization. Due to its large size, the observatory must be folded and stowed to fit within the volume constraints of the fairing of an Ariane 5 launch vehicle. Once on orbit, the observatory (including various optical elements within the OTE) must deploy from its stowed state and the telescope be optically aligned. The stowed and deployed states of the observatory are illustrated in Fig. 1, along with an exploded view of the OTE in which the major components and subsystems are identified for reference. Managing[2,3] the uncertainty in the deployed position of the OTE optical elements, accommodating on-orbit alignment risk, and maintaining the precise alignment of the optics throughout the mission lifetime requires an active optical system with nanometer-level precision and stability for wavefront control.

Webb's primary mirror consists of 18 hexagonal, semi-rigid, light-weighted beryllium mirror segments. The PM segment assemblies (PMSAs) consist of the mirror substrate, a cryogenic hexapod system that provides six degrees-of-freedom adjustment, and a seventh actuator that allows adjustment of the segment's radius of curvature (RoC). These segment-level degrees of freedom allow the segmented PM the flexibility to deploy, align, and phase to act as a monolithic optic. The SM assembly (SMA) consists of a light-weighted beryllium mirror with a cryogenic hexapod system for six degree-of-freedom rigid-body adjustment (the SMA has no RoC adjustment). With a phased PM, the adjustment of the SM is a primary lever in the overall alignment of the telescope on-orbit. In total between the PMSAs and the SMA, there are 132 actuator mechanisms that are used to achieve and maintain the optical alignment of the OTE. In addition to the PMSAs and SMA, the aft-optics subsystem (AOS) contains the light-weighted beryllium TM assembly and the FSM in a beryllium optical bench. Since the alignment of its components are fixed, the AOS is considered the optical alignment reference for the telescope and the PM/SM group are aligned to it on-orbit. The AOS is also aligned and rigidly coupled to Webb's final optical subsystem: the integrated science instrument module (ISIM). ISIM consists of a composite optical bench that supports Webb's science instruments (SIs). While the SIs are all rigidly mounted within the ISIM, all but a single SI contain a focus adjustment mechanism to accommodate minor focus variations either due to the OTE or within the respective SIs. The OTE + ISIM combination (referred to by the acronym OTIS) results in the full optical payload of the Webb Observatory.

1.1 Overview of the Webb mirror actuator and its fine stage

The hexapod assemblies that support and provide six degree of freedom rigid body adjustment of the PMSAs and the SMA are made up of 6 linear actuators assembled in three bipod assemblies, as shown in Fig. 2. The seventh actuator that provides RoC adjustment for the PMSAs is of the same design as the hexapod actuators. Designed by Ball Aerospace, the linear actuators[4] are of a novel single stepper motor-based two-stage design that is capable of sub-10 nm motion accuracy over a 20 mm range both at ambient and cryogenic conditions, as is required for precise control of mirror position after deploying 12.5 mm out of the mirror launch restraints during ground tests and on-orbit.

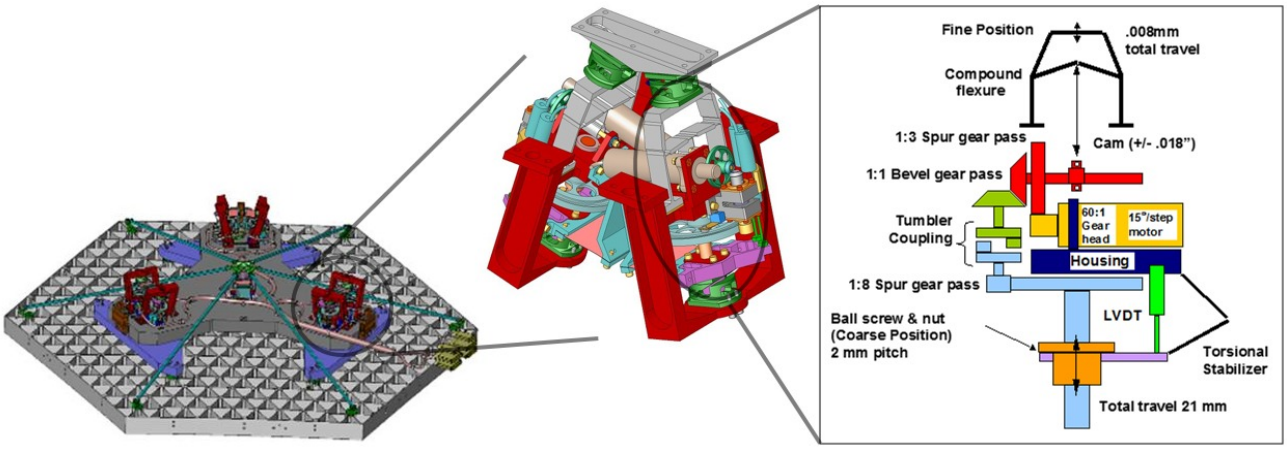

Figure 2. Overview of the PMSA hexapod mounting and the linear actuators. *Left:* Back of a PMSA, showing the six hexapod actuators (located inside of the red brackets). The SMA hexapod is of a similar design. The PMSA RoC actuator is in the center of the PMSA and is attached to the six struts that reach to the edge of the mirror substrate. *Center:* Zoom-in to one of the three bipod assemblies, which shows two individual actuators. *Right:* A cartoon view of the layout of the actuator drive train. Further description is provided in the text.

As shown in Fig. 2, the actuator is driven by a single stepper motor with 24 steps per revolution. This stepper motor drives a resolver and a 60:1 gear head, which further drives a 3:1 spur gear that is attached to an eccentric cam shaft. The cam shaft drives the cross beam of a compound flexure, which deflects the flexure's side beams and further changes the flexure's overall height. The motion reduction of the eccentricity of the cam shaft to flexure height is ~100:1. The eccentric cam shaft and flexure together make up the fine stage of the Webb mirror actuators, with a single rotation of the cam resulting in a near-sinusoidal height change of the actuator. The sinusoidal shape of the linear motion as a function of motor step count is referred to as the "cam profile". The cam profile of this actuator design nominally has a peak-to-valley (PV) range of 10 μm with a step-size of 7.7 nm within the linear zones of the curve, as identified in Fig. 3. Given the gearing from the stepper motor rotation, one period of fine stage motion is equal to 4320 motor steps.

At the end of the eccentric cam shaft is a 1:1 bevel gear that turns a drive shaft into a tumbler-type coupling. This "coarse stage coupler" consists of a rotating disk on both a drive shaft and a driven shaft, each of which has a protruding pin as shown in Fig. 2. This coupling produces an intentional backlash of ~90% of a shaft rotation. When the driving shaft is rotated such that the pins contact, the driven shaft begins to rotate. If the drive shaft's direction is reversed, the shaft can rotate freely until it contacts the driven shaft's pin in the opposite direction. The fine stage flexure can be operated within this ~90% backlash zone without affecting anything further down the drive train, which allows the fine stage motion to be decoupled from the actuator's coarse stage. For coarse stage motion, the driven shaft of the coarse coupler has a spur gear pinion attached, which further drives a large ring gear with an 8:1 ratio. This ring gear drives a threaded shaft on which a ball screw with 2 mm pitch is attached. The resulting axial motion of the ball screw along the threaded shaft makes up the coarse stage of the linear actuator, which has a ~20 mm range and a step size of 0.058 μm. The coarse length change of the actuator is sensed by a linear variable differential transformer (LVDT).

1.2 Actuator fine stage calibration

Due to the hexapod arrangement and two stage actuator design, moving one of Webb's PMSAs or SMA requires a complex set of calculations and strategic planning of actuator motions to precisely achieve a given rigid body pose of the mirror. The calculations and trajectory planning are all handled within the flight Mirror Control Software (MCS), which relies on a set of configuration files to translate desired mirror moves into actual mechanism operations. The static properties of the actuators (i.e., unchanging characteristics of the hardware that are established during acceptance tests) are permanently recorded in the MCS Configuration File, while dynamic properties (i.e., properties that are updated any time an actuator is moved) are continuously updated within the Mirror State Database (MSDB). The dynamic actuator properties that are updated in the MSDB are carefully bookkept and configuration controlled each time an actuator is moved to ensure that the physical state of the actuators is consistent with the state that the software believes it to be in.

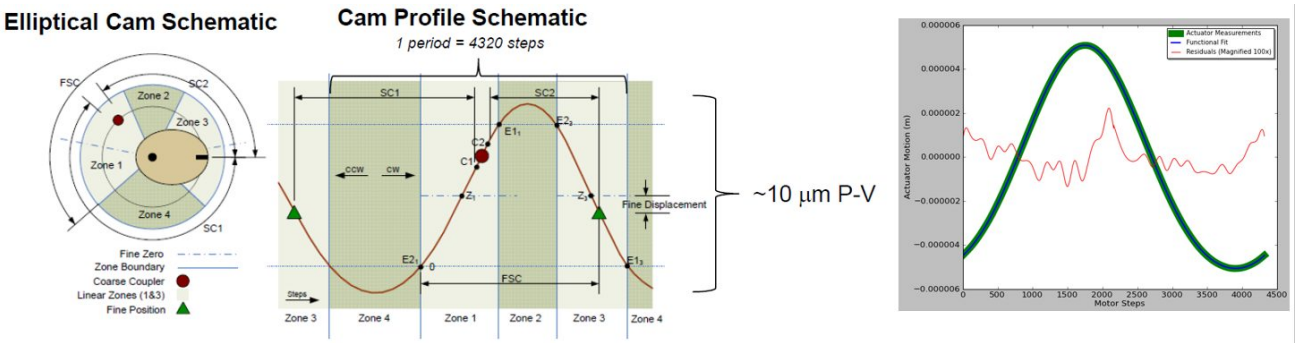

Figure 3. *Left:* Schematic view of the fine stage cam profile curve and how it relates to the location of the elliptical cam position with respect to the coarse coupler. The four zones of the cam profile are shown (where zones 1 and 3 are the linear zones), along with a definition of the FSC and the distances to the coarse coupler in the clockwise (SC1) and counter-clockwise (SC2) directions. *Right:* A plot of the 4320 DMI fine stage calibration data points (green) for the pA4-4 actuator. The modified sine functional fit is shown in blue, with the residuals shown magnified 100x in red. The RMS of the fit residuals is 8 nm.

The hardware properties that are recorded in the MCS Configuration File and the MSDB were established at the actuator-level during acceptance test and calibration activities prior to integration into the PMSA hexapod. Among many measured actuator properties, a primary measurement is to characterize the actuator's motion and assign motor step counts to actuator length. This precise calibration is performed multiple times per actuator at both ambient and cryogenic temperatures using a displacement-measuring interferometer (DMI) in conjunction with specialized ground test software to run the actuator motors. Due to the two-stage design of the actuator, coarse step counts (CSC) and fine step counts (FSC) must be calibrated separately. For the fine stage, the location and size of the coarse coupler in units of FSC must be measured, as well as the FSC values that correspond to the beginning and end of the "linear zones" of the near-sinusoidal cam profile in which the motors will operate when moving within the fine range. A schematic of the cam profile and an example of measured cam profile calibration data are shown in Fig. 3.

Throughout years of test activities at various levels of integration, the Webb actuators have been run through many thousands of motor revolutions and have had their measured and calibrated properties handed off from ground test software to the current flight MCS. Throughout these activities, there are several scenarios in which the dynamic actuator properties in the MSDB could become corrupted (e.g., software error, hardware anomalies, user error, etc.), which could result in a mismatch of motor step count to actuator length. Unlike the fine stage, the actuators' coarse stage motion is monotonic with motor direction, and coarse steps are cross-checked against length measurements made in-situ with the LVDT sensor. The fine stage is reliant on software bookkeeping of FSC to retain accurate length knowledge.

1.3 Fine step count knowledge requirements for Webb commissioning activities

Due to the iterative nature of the wavefront sensing and control (WFS&C) process that is used to align the OTE during Webb's commissioning[3,5] on orbit, some uncertainty in the FSC of each actuator can be tolerated. In extreme cases, a large FSC mismatch between the hardware and the MCS (i.e., on the order of the width of a non-linear zone in the cam profile) can result in an actuator moving the wrong direction within the fine range. A small FSC mismatch, however, will result in a small corresponding length error of the actuator. As tabulated in Table 1 and described below, the tolerance to FSC errors is dependent on the type of actuator:

- PMSA hexapod – The final PM coarse phasing iteration, in which small piston offsets must be applied to nearly-phased PMSAs without introducing tip, tilt, or piston errors, is the OTE commissioning activity that requires the most accuracy in rigid body PMSA positioning. To determine the allowable FSC error for PMSA hexapod actuators, a series of Monte Carlo simulations where PMSA actuator lengths were perturbed during coarse phasing were run. The actuator length uncertainties and the number of actuators affected were reduced until the coarse phasing process closed within its error budget 95% of the time. The results of these simulations indicate that size of the maximum allowed FSC error is dependent on the number of actuators affected. In the extreme case of all 108 PMSA actuators being affected, the maximum allowed FSC error on each to result in a successfully phased PM 95% of the time is ±24 steps. Additional scenarios are provided in Table 1.

Table 1. Allowed FSC errors from a Webb WFS&C point of view, broken down by actuator type.

Actuator Type	Allowed FSC Error
PMSA Hexapod*	±24 steps on ≤108 actuators
	±61 steps on ≤13 actuators
	±104 steps on ≤3 actuators
PMSA RoC	±130 steps
SMA Hexapod	±150 steps

* The allowed FSC error for PMSA hexapod actuators is dependent on the number of actuators over the PM that are found to be in error.

- PMSA RoC – To minimize the number of PMSA-level power corrections that are performed during OTE commissioning, the uncertainty in the power of the PMSA wavefront should be less than ~10 nm RMS. This results in a 0.4 μm length uncertainty in the RoC actuator, which corresponds to knowing the FSC to better than ±130 steps.
- SMA hexapod - The majority of SMA motion during the commissioning process of the OTE are coarse moves, which typically have a 1 μm actuator length uncertainty. For a random group of six actuators in the SMA hexapod with 1 μm length uncertainties, this results in ~2 μrad of tilt (which can be easily compensated for by a tilt of the FSM) and ~0.4 μm of piston error. The latter results in ~10 nm RMS of global focus. To ensure that an FSC error doesn't significantly add to this global focus error, the FSC of each SMA hexapod actuator should be known to better than ±150 steps.

While there are flight contingency procedures for recalibrating the FSC of any of Webb's 132 mirror actuators on-orbit, the processes are time consuming (i.e., on the order of days) and would reduce the time Webb could spend accomplishing its science mission. As a risk reduction exercise, measurements of the FSC errors in each actuator were made during OTE functional testing[6] during the various ground test campaigns in the fully integrated OTIS configuration over the last two years. The following sections describe these tests and their results.

2. PMSA HEXAPOD FINE STAGE TESTING AT AMBIENT

Fine stage testing of the 108 PMSA hexapod actuators was completed as a part of the Center of Curvature (CoC[7]) ambient optical test campaigns that were run both pre- and post-environmental testing of the OTIS at the Space Systems Development Integration Facility (SSDIF) at Goddard Space Flight Center (GSFC) in October 2016 and April 2017, respectively. Given the time constraints of the CoC test campaigns, half of the actuators were tested before OTIS environmental acoustic and vibration testing with the other half being completed after.

2.1 Test description

To measure small PMSA tilts from fine range actuation, a custom deflectometer was used from near the OTE CoC to place two low-power 635 nm laser beams onto two adjacent PMSA optical surfaces and measure the location of the return beams on a common detector. The deflectometer consists of a tripod-mounted SBIG STT-3200ME CCD camera (2184x1472 array; 6.8μm square pixels) on an aluminum mount, which provides stable mounting points for the two lasers. The returned laser spots are imaged directly onto the CCD detector with no fore-optics except for a stack of neutral density filters that are used to reduce the laser intensity to an acceptable level for the 0.12 sec minimum exposure time of the camera. The filter mount features a small tilt relative to the CCD detector surface to minimize diffraction and internal reflection effects. The laser diodes are mounted on kinematic mounts to allow fine adjustment of the return spot locations on the detector. The entire deflectometer head is further mounted on a 3-axis adjustable tripod head for proper positioning of the apparatus relative to the PM. Based on the geometry of the lasers relative to the CCD detector, a simple ray-trace indicates that the deflectometer must be located ~1 m inside of the actual OTE CoC, which is accessed from a large test stand that supports other optical instrumentation for the CoC test (see Fig. 4). In this configuration, the two laser beams are separated by ~0.4 m on the PM optical surface and return with a physical separation of ~7 mm on the deflectometer detector.

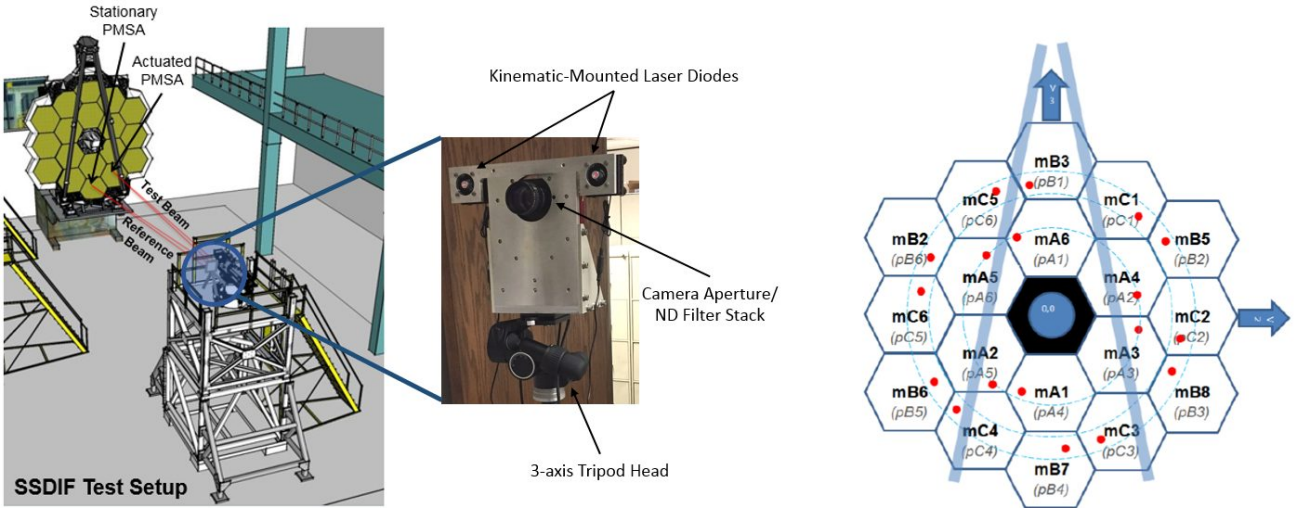

Figure 4. *Left:* Layout of the deflectometer test setup in SSDIF. The deflectometer is setup at the OTE CoC on top of the large test stand. The reference beam and test beam are shown schematically. At right is a front view of the deflectometer head showing the two laser diodes and the camera aperture. *Right:* A view of the pair-wise PMSA test plan for radial laser placement. Red dots indicate the locations of the laser spots on the PM. The dashed circles help visualize common radial distances on the PM. As an example, this figure indicates that segments pB5/pC4 are to be tested together as a PMSA pair.

For one of the two PMSAs with an incident laser beam, one of the six hexapod actuators is stepped through the fine range at regular intervals in time while the deflectometer continuously collects images at ~1 Hz. Via centroid analysis of the "test beam" return spot, the deflection of the test beam off the PMSA surface that is being tilted by the actuator under test is measured relative to the first image. Given the ~15 m distance of the deflectometer to the PM and the pixel size of the CCD detector, the ~10 μm PV range of the actuator fine stage results in ~10 μrad of PMSA tilt, which equates to ~42 pixels of spot motion. By time-syncing the deflectometer image time stamps to the clock kept by the spacecraft simulator (which collects and distributes system telemetry), the deflection distances measured in deflectometer pixels as a function of time can be mapped back to FSC value using telemetry that indicates when the actuator motor completed its fine stage moves. This information is used to create a measured cam profile to which a predetermined periodic function can be fit to recover a measured FSC value that is compared to the value in the MSDB.

The adjacent PMSA on which the second "reference beam" is incident remains stationary during the test to provide a "tilt reference" to track low frequency rigid body movements of OTIS relative to the deflectometer (or vice-versa). Due to the non-spherical sag of the PM surface, the angle of incidence increases with increasing radial position on the PM. For two lasers originating from the same location but reflecting off the PM at different radial positions, rigid body motions of the OTIS would result in similar deflections but with differing magnitudes. That is, the laser at the larger radial distance reflects off a steeper surface than the laser at the smaller radial distance. This effect is minimized by placing both lasers at the same radial distance on the PM, which allows a more accurate subtraction of the motion in the reference beam from the test beam. This necessitated having predetermined segment pairs and laser locations on the PM, as shown in Fig. 4. The need for a reference beam and a validation of the subtraction method was proven in a series of stability tests in which the two laser spots were measured off the PM with no PMSA actuation for a period of 70 mins (approximately the length of time required to test all six actuators of a given PMSA). These tests revealed that high frequency jitter over time scales of ≤30 sec is not correlated between the two beams and is likely due to air turbulence within the SSDIF cleanroom. However, on timescales >30 sec, the correlated drift of the two beams closely track each other which allows successful removal of this signature which would otherwise produce a bias in the FSC measurement. Over the 70 min stability test period, it was shown that correlated drift in the laser spots could be corrected to ~1 pixel RSS, leaving 5.4 pixels 1σ RSS of jitter motion to average over in the FSC measurement.

To start the FSC test, the PMSA under test is pistoned by +0.025 mm (clockwise motor move), which ensures that all six hexapod actuators contact their coarse couplers. This is followed by each actuator being backed off in the counter-clockwise direction by 20 fine steps to separate from the coarse coupler. With the deflectometer properly setup on

PMSAs, background frames are taken for subtraction from the test images, and the deflectometer computer's clock is synced with the spacecraft simulator time. The set of actuator moves to sweep through the fine range is then configured for the test. Here, each actuator is moved through its fine range by moving the actuator motor in the counter-clockwise direction in 30 increments of 130 fine steps, which results in ~90% of the cam profile being swept through for the test. Deflectometer images are collected for 30 seconds prior to the first motor move, and a delay of ~25 seconds is implemented in between motor move commands to allow for deflectometer image collection. At a rate of ~1 Hz, ~25 images are taken per FSC position that can be used to average over the image jitter mentioned previously. This process is repeated for each of the six hexapod actuators on the PMSA under test before swapping the test and reference beams and performing the same test on the adjacent PMSA. Once the first pair of PMSAs are tested, the deflectometer needs to be manually reset on a new PMSA pair before the test can continue. Note that since the deflectometer system is independent of the OTIS spacecraft simulator and ground system software, the data collection is continuous through the fine stage sweep, and the downstream data analysis is relied upon to divide the deflectometer centroids in time into bins corresponding the fine step count. This analysis is described in the following section.

2.2 Data analysis flow

The data analysis for the ambient PMSA hexapod fine stage characterization test is implemented with a series of four Python scripts: a cam profile characterization code, a centroiding code, a telemetry parsing code, and a fitting analysis code.

The cam profile characterization code creates a database of actuator properties that are relevant to the test that were derived from the actuator-level acceptance tests. In particular, this code takes the DMI measured cam profile curve and fits a periodic function to it. The functional form used here is a modified sinusoidal function:

$$length = -\sqrt{A_1{}^2}\,\sin\left[\frac{\pi}{4320}\left(steps + \phi - \frac{4320}{4}\right)\right]^4 + \sqrt{A_2{}^2}\,\sin\left[\frac{\pi}{4320}\left(steps + \phi - \frac{4320}{4} + \frac{4320}{8}\right)\right] + b \quad (1)$$

where A_1, A_2, ϕ, and b are the fitted parameters. The measured FSC value is related to the parameter ϕ. This function provides an excellent fit to the cam profile, with residuals on the order of 8 nm RMS (i.e., similar to the length change for a single fine step; see Fig. 3). In addition, the cam profile characterization code considers the position of each PMSA on the PM, and calculates the expected deflection direction in deflectometer CCD coordinates for a positive actuator length change for all six actuators per PMSA. This information is passed onto the fitting analysis code (described below) as priors to constrain the fit to the deflectometer test data.

The centroiding code performs basic image processing steps (e.g., background subtraction), extracts relevant FITS header information (e.g., image timestamps), and centroids the two laser spots given a set of basic user input (e.g., a lower threshold value). The centroiding is a simple center of mass-type calculation. Typically, the laser spots are highly oversampled and high signal-to-noise ratio as shown in Fig. 5, so the calculated centroid positions are very accurate. The centroid code outputs a data file that is later ingested into the fitting analysis code (see below).

The telemetry parsing code reads in engineering telemetry data from the ground system and parses it to determine the times at which the fine stage sweep motor moves completed. Telemetry is recorded at a rate of 1 Hz on the spacecraft simulator's solid-state recorder (SSR). This code outputs a data file with 30 time stamps corresponding to the times at which the 30 fine stage moves were completed. This information is passed along to the fitting analysis code to be used for binning the deflectometer images into fine step count bins. Note that there are known latencies in the ground system, such that a motor move is reported in the telemetry as being completed after the motor is physically finished moving. For the data to be processed on-board and recorded in the SSR, this delay is ~3 sec, but can vary by ±1 sec depending on when the motor move completed relative to the SSR data rate. This variable delay will be accounted for in the fitting analysis code.

Using a set of laser spot centroids (for both the test beam and the reference beam), centroid timestamps, motor move completion time stamps, cam profile fit coefficients, the expected direction of test beam deflection on the CCD detector, and the starting FSC value from the MSDB, the fitting analysis code determines the FSC error (i.e., the difference between the starting FSC value from the MSDB and the actual starting FSC of the actuator). First, the correlated drift is removed from the test beam centroids by subtracting the reference beam centroids, as shown in Fig. 5. The reference beam centroids are smoothed via 25 image running average to minimize the impact of the high frequency jitter. In addition, the corrected test beam centroids are zeroed out by subtracting the mean centroid position of the first 25 images. All centroids are then relative to this location. Next, a line is fit to the centroid data to measure the exact

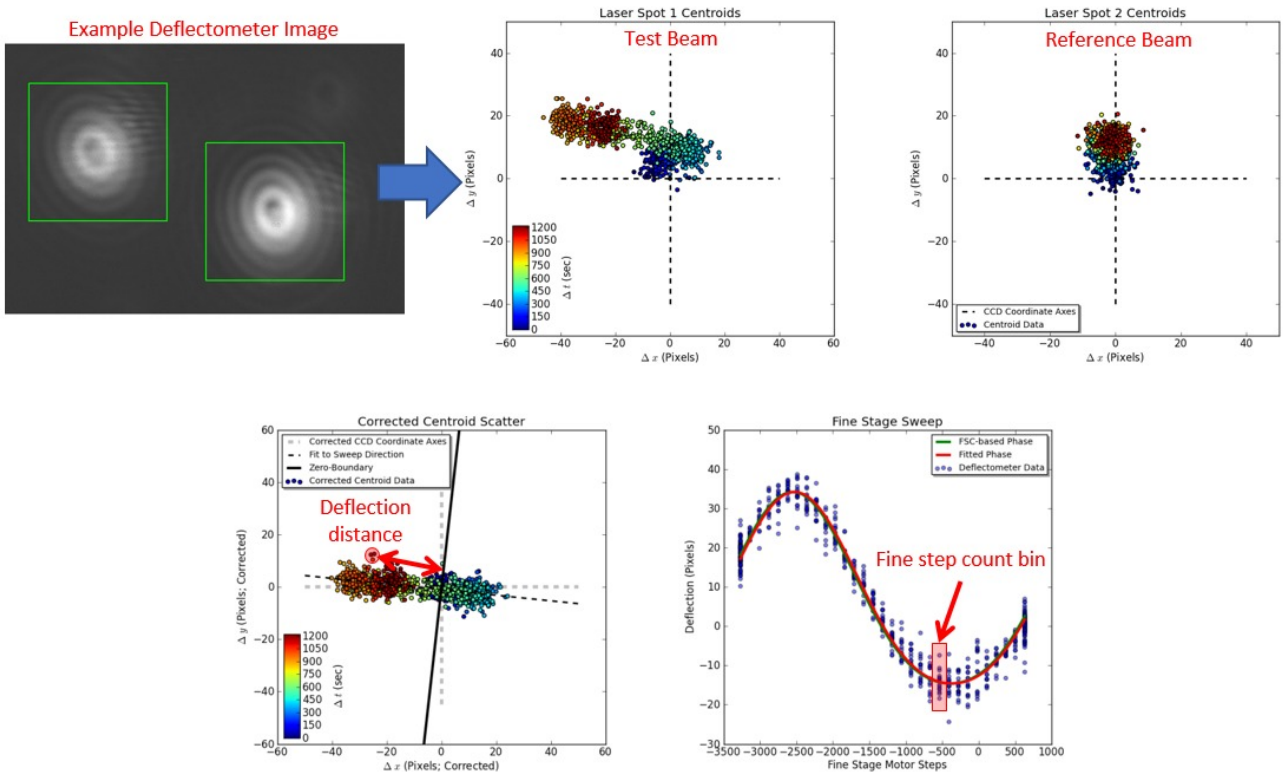

Figure 5. Example data analysis for deflectometer data for actuator pB3-1. From left to right, the top row shows an example deflectometer CCD image, followed by scatter plots of the centroids for the test beam and the reference beam. The data points are color coded by time in sec. At lower left, the drift corrected test beam centroids are shown, along with the fit to the deflection data (dashed line) and the perpendicular "zero-line" (solid line). The deflection distance for an example data point is indicated. At lower right is the deflection data binned into fine step count. Each bin contains ~20 deflection data points. The green curve shows where the curve should be given the MSDB-reported starting FSC value. The red curve is the fit to the deflectometer data. Here, the FSC error $\Delta\phi$ is a modest -26 steps.

direction of deflection, and a line perpendicular to this fit is calculated with its intercept at the origin. The perpendicular line serves as the "zero-line" separating positive and negative deflections, with the positive direction being known from the expected direction calculated by the cam profile characterization code. The distance along the deflection direction from this zero-line is calculated and given a positive or negative direction accordingly, as shown in Fig. 5. Next, the signed deflection distance values are separated into fine step count bins according to the motor move completion times from the telemetry. To avoid improperly binning the deflection data due to the known latency in the telemetry, the first five time-sorted data points are deleted from the bin, leaving ~20 data points per fine step count bin. The sinusoidal function in Eq. 1 is then fit to the binned deflection data using scaled versions of the amplitude coefficients (A_1 and A_2) and the vertical offset (b) that were fit to the actuator DMI data as initial guesses. The least squares fitting code then finds the best-fit values of A_1, A_2, b, and the phase ϕ for the measured deflection data. Using the phase value from the DMI cam profile ϕ_{DMI} and the phase value from the fit to the deflectometer ϕ_{fit}, the fine step count error is derived as $\Delta\phi = \phi_{fit} - \phi_{DMI}$. The measured starting FSC value is therefore $FSC_{fit} = FSC_{MSDB} + \Delta\phi$, where FSC_{MSDB} is the starting FSC value from the MSDB. Example fits to the binned deflection data are shown in Fig. 5.

2.3 Estimation of fine step count uncertainty

The uncertainty on $\Delta\phi$ from this test is estimated from a 10,000 trial Monte Carlo simulation of the previously described analysis, starting with a set of noise-free centroid data that are created based on the cam profile of a randomly selected PMSA hexapod actuator. Noise is added to the centroids to account for CCD signal-to-noise ratio, as well as to reflect the jitter and drift environment within SSDIF that was measured from stability tests. The mock centroid data properly reflect the camera data collection cadence, the time between motor move commands, and the number of fine step

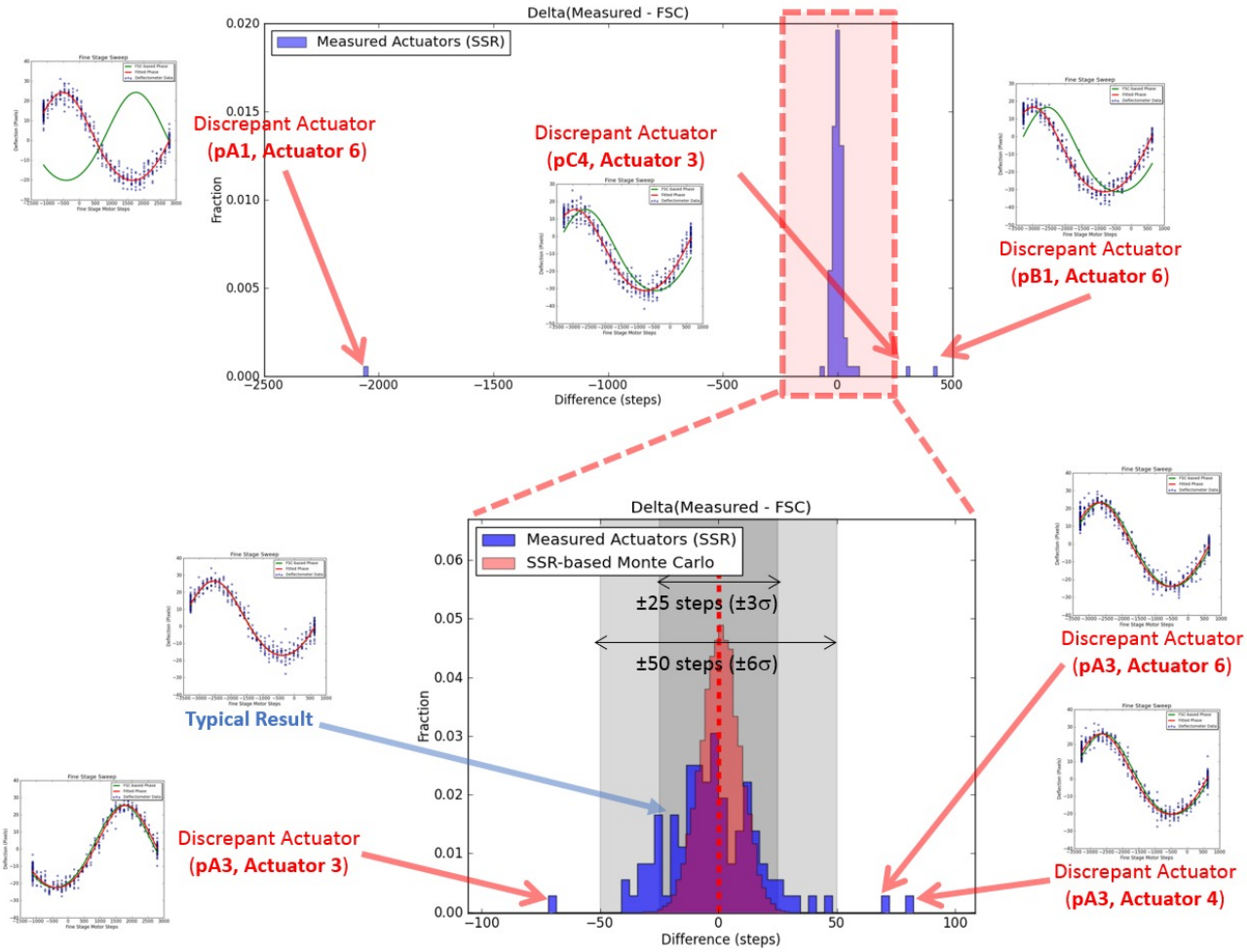

Figure 6. Summary of PMSA hexapod actuator fine step count errors measured with the deflectometer for the entire PM. The top histogram shows all measured actuators. Most of the actuators are centered on a measured FSC error of 0 steps and are grouped into a tight distribution. The lower histogram zooms into this core distribution. The red histogram is the Monte Carlo-derived distribution for 10,000 simulated actuators with no FSC error to illustrate the expected test uncertainty. The blue histogram is for the measured actuators. Actuators that are identified as having large FSC errors in need of correction are highlighted in red, with subplots showing the fits to the deflectometer data. A typical fit result with no measurable FSC error is also shown, highlighted in blue.

intervals that were sampled in the test. In addition, the simulation considers uncertainty in the time synchronization between the deflectometer and the ground system, uncertainty in the motor move completion times due to telemetry sampling, and the variability in the telemetry latency. Based on this simulation, the 3σ (99.7% confidence) uncertainty in the measured FSC error is ±25 steps. The Monte Carlo-derived distribution of measured FSC errors in the scenario where no actuator has lost steps is shown along with the measured FSC error distribution (results discussed in the following section) in Fig. 6.

2.4 Summary of PMSA hexapod actuator fine step count errors

Fig. 6 shows histograms that summarize the measured FSC errors for all 108 PMSA actuators. Immediately noticeable are the three clearly discrepant actuators (pA1-6, pC4-3, and pB1-6). Excluding these actuators, the remaining 105 actuators reside in a relatively tight distribution that is centered around an FSC error of 0 steps. This core distribution is also shown in Fig. 6 and is plotted along with the expected distribution from the Monte Carlo uncertainty estimate. There are 26 total actuators that lie outside of the ±3σ test uncertainty limit.

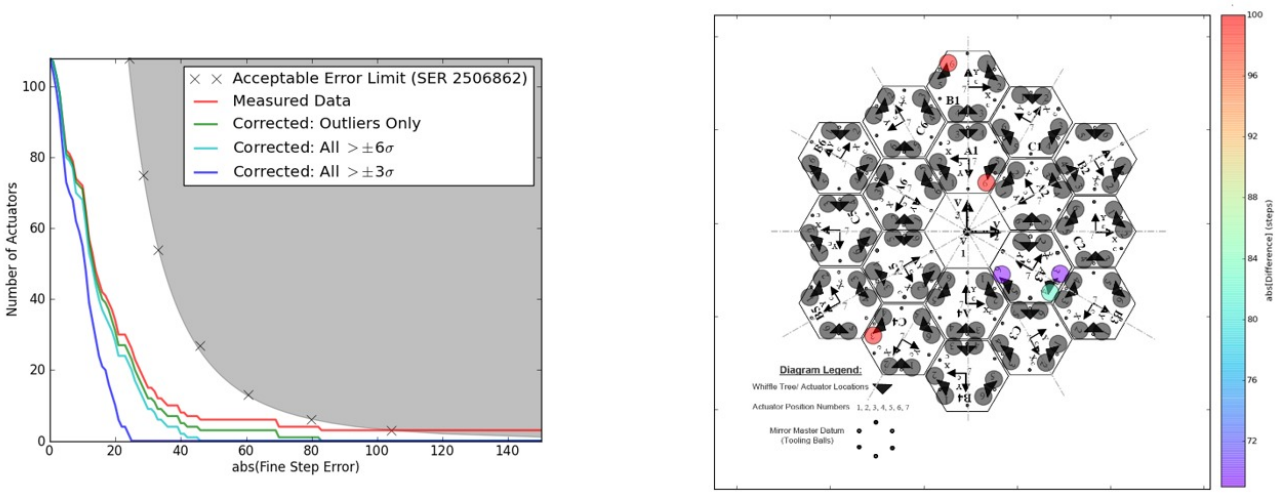

Figure 7. *Left:* Plots of FSC error cumulative distributions for the initial deflectometer measurements (red), for correction of the largest three FSC errors (green), for correction of all actuators outside of the ±6σ detection limit (cyan), and for all actuators outside of the ±3σ detection limit (blue). The gray region of the plot indicates the space where the number of actuators with FSC errors of a given size would cause the coarse phasing process to fail at least 5% of the time. *Right:* A map of the PM showing the six actuators whose FSC values were updated in the MSDB because of the deflectometer testing. The color of the data point representing a given actuator corresponds to the size of the FSC correction issued.

As previously mentioned, roughly half of the actuators were tested prior to the acoustic and vibration environmental testing of OTIS, with the other half tested after. To check for any effects that these environmental tests had on the actuator's ability to mechanically maintain their fine step count, the distribution of actuators tested pre-environmental was compared to the post-environmental distribution. A 2-sample KS test was implemented on these two distributions and found that they are statistically indistinguishable (test statistic of 0.138 with a *p*-value of 0.693). In addition, four actuators were tested both pre- and post-environmental testing, with all four actuators having the same measured FSC errors in both tests within the Monte Carlo-based measurement uncertainty. These results clearly indicate the actuators' resilience to launch conditions.

2.5 Fine step count corrections

Requirements for the maximum allowed PMSA hexapod FSC errors were discussed in Section 1.3 and in Table 1. From the coarse phasing Monte Carlo simulation, the relationship between the number of actuators with a given FSC error as a function of the size of the FSC error is shown in Fig. 7. The gray region of that plot represents the un-allowed space occupied by too many actuators with too large of FSC errors that would result in the coarse phasing process failing its requirements at least 5% of the time. The four colored curves in the plot are cumulative distributions of the PMSA actuator measurements. The red curve represents the initial measurements that were summarized in Fig. 6. As can be seen the red curve crosses into the gray space due to the three actuators with the largest FSC errors. If only these three actuators FSC values were corrected in the MSDB using the measured value, the resulting cumulative distribution would be represented by the green curve, which produces an acceptable ensemble PMSA actuator state from a WFS&C standpoint. The cyan curve shows the cumulative distribution if all actuators outside of the ±6σ detection limit have their FSC values corrected (this consists of the six actuators identified in red in Fig. 6), while the blue curve represents the cumulative distribution if all actuators outside of the ±3σ detection limit being corrected.

Correcting an actuator's FSC value requires hand-editing the flight MSDB, which is prone to human error. As a middle ground approach, it was decided that only the six actuators outside of the ±6σ detection limit would have their FSC values corrected, which results in the cyan cumulative distribution shown in Fig. 7. The locations of these six actuators on the PM are also shown in Fig. 7. As a spot-check on the procedure for editing the MSDB for these actuators, fine stage testing was repeated for actuators pB1-6 and pA1-6 using the deflectometer. After correction, the measured FSC errors for these two actuators was measured to be 32 steps and 4 steps, respectively. Note that the uncertainty in these two measurements is ±36 steps at 3σ, which considers not only the measurement uncertainty of the measurement itself,

but also the uncertainty in the applied correction based on the initial measurement. This indicates that the procedures for updating the MSDB's FSC values is robust.

3. PMSA HEXAPOD ACTUATOR FINE STAGE CROSS-CHECKS AT CRYO

Optical testing of OTIS in a simulated space environment took place within Chamber A at Johnson Space Center (JSC) over the summer of 2017 (see Ref. 8). For reference, a schematic view of the Chamber A test setup is shown in Fig. 11 later in this paper, with subsystems that are relevant to actuator fine stage testing identified. For additional tests of the PMSA hexapod actuators that were intended to act as a cross-check to the deflectometer measurements at ambient, the Center of Curvature Optical Assembly's (COCOA[9]) multi-wave interferometer was used to measure PMSA surface tilts. As its namesake implies, COCOA is a set of optical instruments that are placed within Chamber A above OTIS at the OTE CoC. COCOA's primary use is to provide measurements that guide the cryo-alignment of the PM during test and to provide a means to measure the wavefront error of the aligned PM to verify observatory-level requirements.

3.1 Test description

PMSA hexapod actuator fine stage testing took place during cryo-stable conditions and started with the PM in a stacked and phased state. In such a state, the COCOA interferometer can measure segment-level tilts across the entire PM simultaneously such that a single actuator for several PMSAs can be tested at once. Due to time constraints in the cryo-vacuum test environment, a single actuator on 8 different segments were chosen to be tested, with the remaining 10 segments acting as tilt references. For each COCOA measurement taken, the measured tilt of the 8 segments under test is calculated relative to the average of the 10 stationary segments. Two COCOA interferometric measurements are taken per fine step count interval.

Like the ambient fine stage tests, each of the 8 actuators under test were driven in the counter-clockwise direction until contact with the coarse coupler is made. A set of COCOA interferometric measurements are taken at that point as the baseline measurement, then the actuators under test are stepped by 130 fine steps in the clockwise direction. Again, a pair of COCOA interferometric measurements are made. The 130-step move followed by a COCOA measurement is repeated 29 more times to cover 3900 fine steps, or ~90% of the period of the fine range cam profile. The process of completing the mirror move and taking the COCOA measurements takes ~9 minutes to complete per measurement, resulting in a ~4.5 hour-long test.

3.2 Data analysis flow

The COCOA team reduces the measured interferograms to produce a set of orthogonal tilt measurements in units of μrad for each of the 8 segments under test relative to the 10 stationary segments. Unlike the deflectometer testing, the COCOA data collection process was not continuous through the fine stage moves. As such, given the starting FSC value reported through the MCS, the fine step count at each of the 31 COCOA measurements is immediately known without the need for parsing motor move telemetry. Thus, the sinusoidal function in Eq. 1 can be fit directly to the COCOA tilt data to determine $\Delta\phi$ as described in Section 2.2. An example of the fit to the COCOA measured tilts for one of the 8 segments under test is shown in Fig. 8.

3.3 Estimation of fine step count uncertainty

Like with the deflectometer analysis, a Monte Carlo simulation is used to estimate the cumulative effect of the various measurement uncertainties on the uncertainty of the fitted FSC error. For the cryo PMSA hexapod fine stage characterization tests, two main sources of uncertainty are at play. First, there is error in the tilt measurements by COCOA, which is largely due to signal to noise in the interferograms. Since two back-to-back COCOA measurements were made per fine step count interval during the test, the standard deviation of the difference between two the measurements over the 31 fine step count intervals was used as an estimate of COCOA measurement uncertainty. This is quite small at a 1σ difference of 0.02 μrad RSS. The second, more dominant error source considered is due to thermal effects associated with the ground test setup within Chamber A. Due to a known mechanical short between the OTIS and the ISIM's electronics compartment, an oscillatory thermal load is applied to the PM backplane assembly as one of the electronics heaters is cycled. The cycle period is ~28 minutes, which causes a tilt oscillation in the PMSAs on the same timescale. The magnitude and direction of the tilt varies from PMSA to PMSA, making this source of uncertainty uncorrectable. Using the tilt data from the 10 reference segments, the range of magnitudes and directions of the tilt

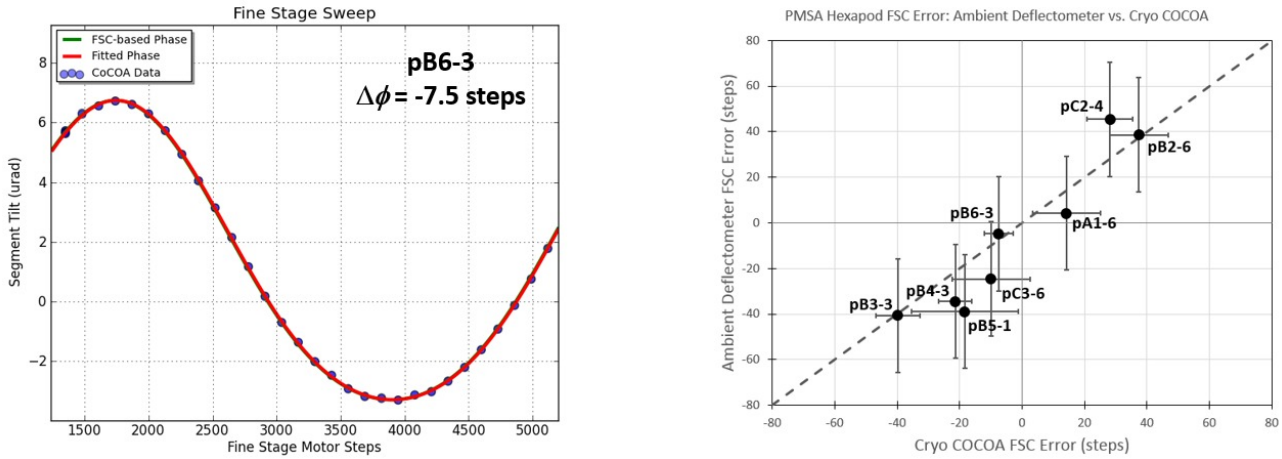

Figure 8. *Left:* An example of the COCOA-measured tilt data for the fine stage characterization test of pB6-3at cryo. *Right:* A comparison of the COCOA-measured FSC errors at cryo for the 8 actuators to the deflectometer-measured FSC error at ambient. The dashed line shows the 1:1 relation. The 3σ error bars for each of the 8 actuators overlaps with the 1:1 line indicating generally excellent agreement between the two measurements.

oscillations can be estimated and modeled in the Monte Carlo simulation. The typical PV tilt oscillation is only 0.18 μrad with a standard deviation of 0.08 μrad. These error sources are insignificant compared to the ~10 μrad PV of the segment tilt due to the fine stage of a given actuator. The resulting uncertainty in the FSC error measured with COCOA is typically only ±9 steps (3σ).

3.4 Comparison of PMSA hexapod actuator cryo fine step count errors to the ambient test results

A comparison of the 8 PMSA hexapod actuators measured with COCOA compared to the deflectometer measurement at ambient is provided in Fig. 8. With 3σ error bars shown, this plot illustrates the generally excellent agreement between the FSC error measured at cryo compared to the independent measurement made at ambient. As such, the cross-check of the deflectometer measurements provided by COCOA yields a great deal of confidence in the ensemble FSC error measurement distribution presented in Section 2.4 for the 108 PMSA hexapod actuators.

4. PMSA RADIUS OF CURVATURE ACTUATOR FINE STAGE TESTING AT CRYO

Since changing the RoC of the PMSA optical surface results in a change of power in the measured wavefront, COCOA is also used to perform fine stage characterization testing for the 18 PMSA RoC actuators.

4.1 Test description

PMSA RoC actuator fine stage testing took place during cryo-stable conditions and started with the PM in a stacked and phased state. In such a state, the COCOA interferometer can measure segment-level power across the entire PM simultaneously such that the RoC actuator for 9 PMSAs can be tested at once, with the remaining 9 segments remaining stationary for reference. Here, the 9 odd-numbered segments were tested first, followed by the 9 even-numbered segments. For each COCOA measurement taken, the measured change in power is translated to a change of the sag of the mirror surface for the 9 segments under test is calculated. Two COCOA interferometric measurements are taken per fine step count interval. Note that the ~10 μm PV change in length of the PMSA RoC actuator fine range results in a ~500 nm PV change in sag of the PMSA optical surface.

Like the ambient fine stage tests, each of the 9 actuators under test were driven in the counter-clockwise direction until contact with the coarse coupler is made. A set of COCOA interferometric measurements are taken at that point as the baseline measurement, then the actuators under test are stepped by 130 fine steps in the clockwise direction. Again, a pair of COCOA measurements are made. The 130-step move followed by a COCOA measurement is repeated 29 more

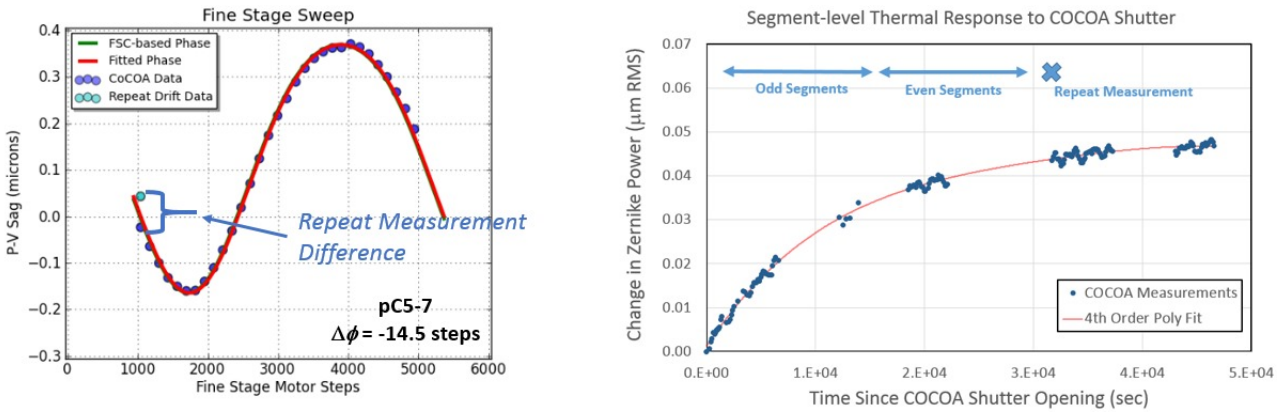

Figure 9. *Left:* An example of the COCOA-measured PV sag data for the RoC fine stage characterization test of pC5. The uncorrected FSC error is measured to be -14.5 steps. Note the significant difference in the repeat measurement and the systematically poor fit to the data. A corrected version of this measurement is shown in Fig. 10. *Right:* The segment-level thermal response to the COCOA shutter being open measured as power as a function of time since the shutter opened. For reference, the length of time of the RoC fine stage characterization tests for each set of segments plus the repeat measurement are shown to illustrate the expected change in segment-level power over the course of the test.

times to cover 3900 fine steps, or ~90% of the period of the fine range cam profile. The process of completing the mirror move and taking the COCOA measurements takes ~9 minutes to complete per measurement, resulting in a ~4.5 hour-long test. Once completed for the first 9 RoC actuators, the test is repeated for the other 9 actuators. To finish the test, all 18 actuators are driven counter-clockwise back to the starting FSC value and another pair of repeat COCOA measurements are collected. This is for characterizing any thermal drift in the segment-level power due to the thermal load from the COCOA shutter having been open for several hours during the test.

4.2 Data analysis flow

The COCOA team reduces the measured interferograms to produce a set of PV sag measurements for each segment in units of µm. Since there is a single pair of COCOA measurements collected for each fine step count interval, the fine step count at each COCOA measurement is known without the need for parsing motor move telemetry. As with the cryo PMSA hexapod fine stage characterization test, the sinusoidal function in Eq. 1 can be fit directly to the COCOA sag data to determine $\Delta\phi$ for the RoC actuators as described in Section 2.2.

Inspection of the repeated measurements at the starting FSC value that are separated in time by the test duration shows that they generally do not match, differing by ~0.05 µm sag for odd segments and ~0.01 µm sag for even segments. Additionally, fitting Eq. 1 directly to the raw data typically results in a poor overall fit, with the measured cam profile appearing to be "stretched" relative to the best-fit curve. These differences are illustrated in Fig. 9, and are due to thermal loading of the PMSAs because of COCOA's shutter being open during the lengthy RoC fine stage characterization test period. This known thermal response of Zernike power was measured during the OTIS cryo-vacuum test for the entire PM and is shown scaled to the segment-level in Fig. 9 along with a best-fit fourth order polynomial that applies for times up to 12 hrs after the COCOA shutter is opened. To correct for this effect, the thermal response curve is first re-zeroed according to the time since the COCOA shutter was opened: this time is ~0.5 hrs for the odd-numbered segments and ~5 hrs for even-numbered segments. Next, since each PMSA may see a different thermal load from the COCOA shutter (e.g., due to shadowing from the SMA support struts), a scale factor is applied to the thermal response curve. Since the time relative to the opening of the COCOA shutter is known for each of the COCOA fine stage characterization measurements, the resulting power drift due to the thermal load can be subtracted from the data. When fitting the cam profile curve, the thermal drift scale factor is allowed to vary, where the adopted value corresponds to the minimum in the fit uncertainty on the phase parameter ϕ of Eq. 1. When the adopted drift scale factor is applied to the thermal response curve and subtracted from the fine stage characterization data, the initial COCOA measurement and the final repeat measurement typically agree with each other to within ~6 nm in PV sag, which is on the order of the COCOA measurement uncertainty. An example of the best-fit cam profile to the COCOA measurements for the RoC fine stage characterization after the thermal drift has been corrected for is shown in Fig. 10. In addition, Fig.

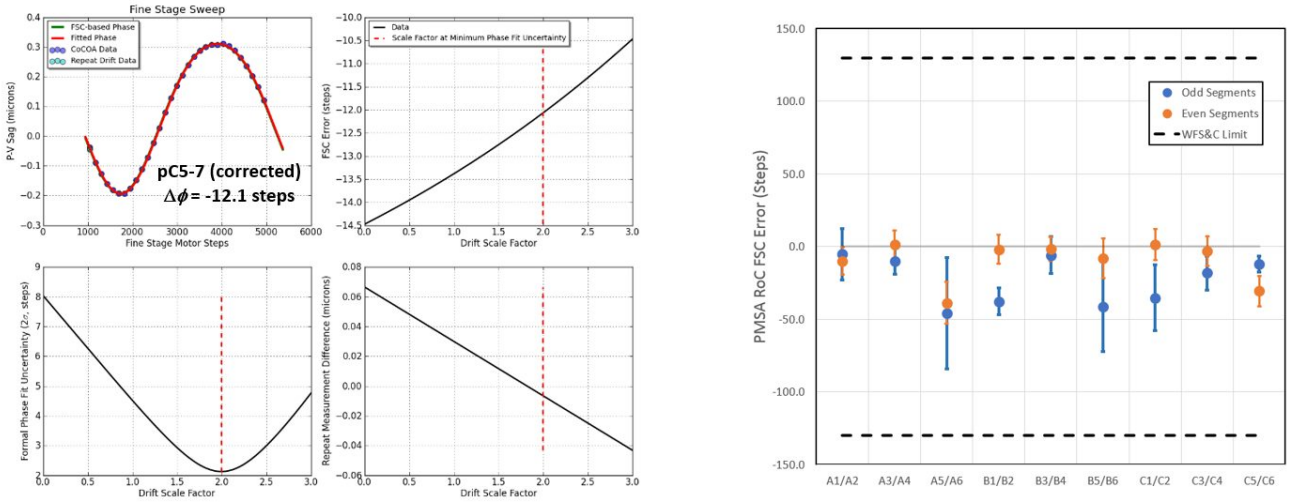

Figure 10. *Left:* A set of four plots showing the fit to the pC5 RoC fine stage characterization data after correction for the COCOA shutter thermal effects. The corrected FSC error is -12.1 steps. The lower left plot shows the fit error in ϕ as a function of drift scale factor. The plot at lower right shows the repeat measurement difference as a function drift scale factor. The plot at upper right shows the measured FSC error as a function of drift scale factor. In the latter three plots, the vertical dashed red line indicates the best-fit drift scale factor that was used to correct the data. *Right:* A summary plot of all 18 RoC actuators' measured FSC errors and 3σ uncertainties relative to the WFS&C-determined FSC error limit.

10 shows the fit uncertainty on ϕ, the measured FSC error, and the difference between the COCOA repeat measurements as a function of the drift scale factor.

4.3 Estimation of fine step count uncertainty

Uncertainty in the measured FSC error for the RoC actuators consists of the variance in the parameter estimate of ϕ from the non-linear least squares fitting algorithm, as well as a separate systematic component. The ϕ parameter variance was also minimized to determine the thermal drift scale factor (see the lower left plot in Fig. 10). Since there is not much scatter in the COCOA measurements, this uncertainty on the order of only ±3 steps at 3σ for the best-fit thermal drift factor. A systematic component is also carried through into the final error bar to account for uncertainties in the thermal drift scale factor since the response of each individual PMSA was not directly measured. To be conservative, the uncertainty is assumed to be equal to the difference between the FSC error measured with the corrected data and that measured from the uncorrected data set. At maximum, this difference is 35 steps for segment pA5. The straight sum of the uncertainty in ϕ and the systematic component makes up the full error bar associated with each measurement.

4.4 Summary of PMSA RoC actuator fine step count errors

A summary of the PMSA RoC actuator FSC errors measured with COCOA is shown in Fig. 10 relative to the acceptable FSC error limits set from a WFS&C perspective. As can be seen, all 18 RoC actuators lie safely within the acceptable FSC error limits even when considering the conservative systematic uncertainty estimation associated with the thermal drift factor.

5. SMA ACTUATOR FINE STAGE TESTING AT CRYO

The "pass-and-a-half" (PAAH[8,10]) optical test is a part of OTIS cryo-vacuum testing at JSC and is the only end-to-end optical test of the Webb telescope. In this configuration (shown schematically in Fig. 11), the AOS Source Plate Assembly (ASPA) is used at the intermediate Cassegrain focus of the OTE to inject light into the optical system towards the SMA. The SMA reflects the light to the PM, which nominally collimates the beam. In Chamber A above the OTIS are three 1.5 m diameter Auto-Collimating Flat (ACF) mirrors that sparsely sample the OTE pupil and each straddle the intersection of three PMSAs, as shown in Fig. 11. The collimated light reflects off the ACFs back towards the 9 PMSAs

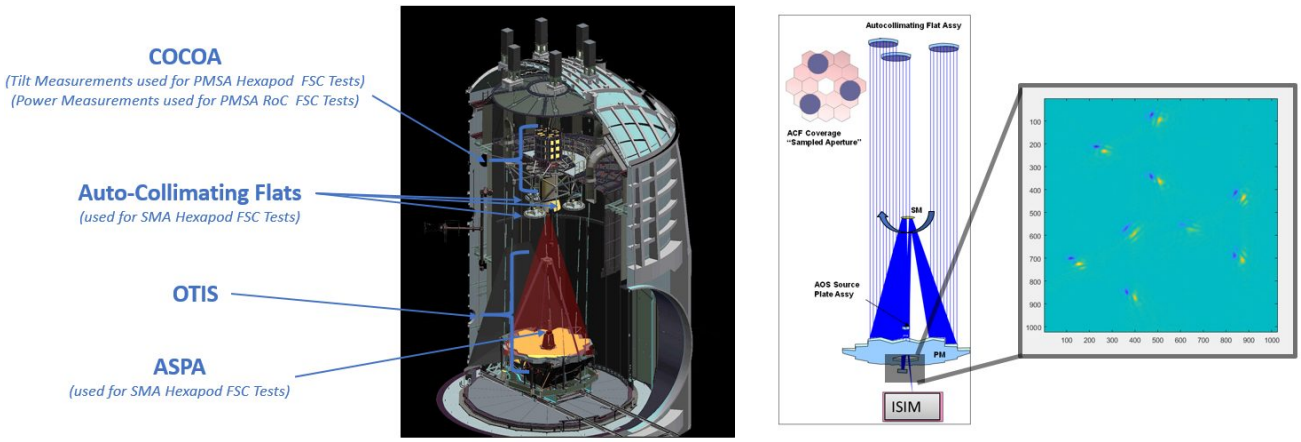

Figure 11. *Left:* Schematic cut-away view of JSC's Chamber A as it was configured for the OTIS test. The main subsystems as they apply to fine stage characterization testing are identified. *Right:* An optical diagram of the OTIS PAAH test setup in which the location of the ACFs within the OTE pupil is also shown. The image at right shows the difference between two PAAH Hartmann images produced by an optical model in which a shift of ~50 pixels in a NIRCam shortwave channel for all 9 PSFs is shown for a tilt of the SMA produced by actuating a single SMA hexapod actuator through its PV fine range of motion.

and through the entire OTIS optical train. The ASPA source is finally reimaged onto one of the SIs within ISIM. In this configuration, small tilts of the SMA result in movement of the image at the SI focal plane.

5.1 Test description

The SMA fine stage characterization data were taken as a part of PAAH optical testing under cryo-stable conditions with the SMA at its best-focus position and in a configuration known as the Hartmann "small array" (see Ref. 10). In the small array, the ACFs and the PMSAs under them are unstacked and tilted off to create 9 distinct PSFs: one from each PMSA, as shown in Fig. 11. Images of the ASPA on-axis source at a wavelength of 2.12 μm are captured in the NIRCam B shortwave channel. For the SMA hexapod actuators, the ~10 μm PV fine range corresponds to a tilt of the SM by ~15 μrad (compared to a PMSA, this tilt is larger for the same actuator length change due to the smaller footprint of the bipods on the back of the mirror substrate). For the NIRCam B shortwave detector, the above tilt equates to a deflection of ~50 pixels after traversing the PAAH optical path. Over these small angles, each of the 9 small array PSFs should deflect by a similar amount.

Like the other fine stage tests, each of the SMA hexapod actuators were driven in the counter-clockwise direction until contact with the coarse coupler is made. A NIRCam B image is then taken as the baseline measurement for the fine stage characterization test of the first hexapod actuator. The first actuator under test is then stepped by 325 fine steps in the clockwise direction away from the coarse coupler, followed by the collection of another NIRCam B image. The 325-step move followed by a NIRCam B image collect is then repeated such that 3900 fine steps have been stepped through. The final image in the first actuator's test serves as the baseline image for the next actuator's test. The process is repeated for the remaining 5 hexapod actuators.

5.2 Data analysis flow

The deflection of the 9 small array PSFs is measured from the 13 NIRCam B images for each actuator (1 baseline image plus 12 fine step count intervals) via centroid analysis using a tool[10] that was developed specifically for the various parts of PAAH Hartmann testing. The direction of the deflection in local detector coordinates for a positive length change of each SMA hexapod actuator is determined from an optical model. Using this information, the deflection distance is calculated using the same fitting analysis code that was used for the PMSA hexapod fine stage characterization testing at ambient with the deflectometer. Given the starting FSC value reported through the MCS, the fine step count at each of the 13 centroid positions is known. Thus, the sinusoidal function in Eq. 1 can be fit directly to the NIRCam B centroids to determine $\Delta\phi$ as described in Section 2.2. Since each NIRCam B image contains 9 PSFs on which to centroid, the fit is performed 9 times to result in 9 $\Delta\phi$ values, the average of which is taken to be the FSC error for the actuator. An

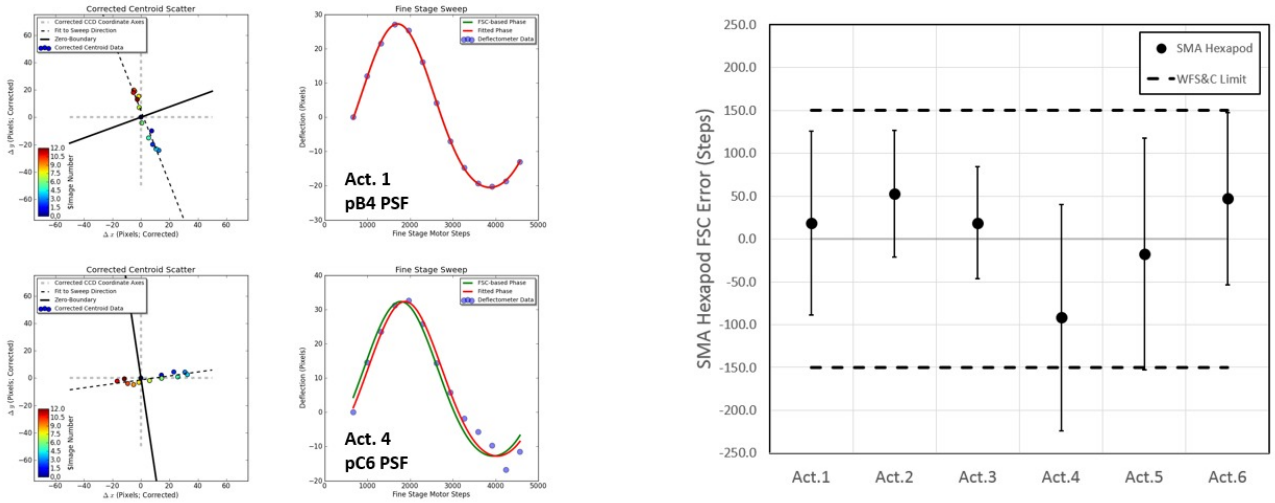

Figure 12. *Left:* Example SMA hexapod actuator fine stage characterization test data. The top row shows the deflection data and resulting cam profile fit for actuator 1 using the pB4 PSF. Since the deflection direction of this actuator is oriented along the y-direction of the NIRCam B detector, it is minimally affected by the x-oriented common mode motion. In contrast, the same is shown below for actuator 4 using the pC6 PSF (note the distorted trough of the measured cam profile). *Right:* Summary of the FSC errors measured for the SMA hexapod actuators compared to the WFS&C-based limits (dashed lines). The error bars are shown on the data points are 3σ.

example of the fit to the deflection distances calculated from NIRCam B centroids for SMA hexapod fine stage actuator testing is shown in Fig. 12.

5.3 Estimation of fine step count uncertainty

Since the SMA fine stage characterization test measurement is ultimately a mean of measurements made from 9 different PSFs, test uncertainties can be estimated in-situ by simply taking the standard error in the mean of the 9 individual FSC error measurements. While such a method captures random uncertainties from the PSF-to-PSF measurements, it does not capture systematic effects that have an impact on all 9 PSFs collectively. Such common-mode effects are not correctable in this test due to a lack of a reference. Stability testing with NIRCam imagery to assess the dynamics of the test environment in the PAAH configuration was conducted at the beginning of the cryo-stable phase using the same exposure parameters as the SMA fine stage characterization test. The stability testing identified cyclical global motions common to the 9 PSFs, primarily along the x-axis in local NIRCam B detector coordinates, with a PV motion of ~12 NIRCam B shortwave pixels. This uncorrectable effect will most negatively affect the data for actuators 4 and 5, whose orientation in the SMA hexapod orients the deflection primarily along the NIRCam B shortwave x-direction. This effect is shown in Fig. 12.

To estimate the resulting uncertainty on the FSC error measurement due to the uncorrectable common-mode motions in the system, a Monte Carlo simulation was run for each individual actuator in which the measured stability data was used to inject the common mode motion on top of an ideal set of NIRCam B shortwave centroids that were produced based on the DMI-measured cam profiles for each actuator and the expected direction of deflection within NIRCam B's shortwave channel. For each Monte Carlo trial, a random point in time within the stability data was chosen as the starting point, and the time sampling was varied within the range of differences in time at which the NIRCam B images were acquired during the fine stage characterization testing. For each Monte Carlo trial, the simulated deflections with superposed common-mode motion were fit to measure the resulting FSC error. Based on this method, the systematic FSC error uncertainty is estimated to range from ±55 to ±132 steps at 3σ, with the largest uncertainties corresponding to actuators 4 and 5 as expected. In contrast, the FSC error measured among the 9 PSFs for each actuator are quite repeatable with a 3σ uncertainty (averaged across the six actuators) of only ±13 steps. For the total error bar, the systematic error from the uncorrectable common mode motion is summed with the standard error estimated from 9 individual FSC error measurements for each actuator.

5.4 Summary of SMA hexapod actuator fine step count errors

A summary of the SMA hexapod actuator FSC errors measured in the PAAH test configuration is shown in Fig. 12 relative to the acceptable FSC error limits set from a WFS&C perspective. Except for actuators 4 and 5, the SMA actuators lie safely within the acceptable FSC error limits. Actuator 4 was measured to have the largest FSC error of all six SMA actuators at -92 steps. However, due to its orientation on the hexapod, its deflection is in the same direction as the uncorrectable common-mode drift, which maximizes the resulting uncertainty in the FSC error measurement. The latter is also true for actuator 5. As a result, the large error bars for these two actuators cause them to slightly exceed the FSC error limits.

If in fact actuators 4 and 5 have FSC errors that lie at the extreme lower end of their 3σ uncertainty range such that they exceed the FSC error limits estimated from a WFS&C perspective, the resulting effect on the alignment and commissioning process of the OTE is not significant as the SMA hexapod is the most forgiving of the three actuator types to FSC errors. Ultimately, if one is willing to accept more than a single iteration of SMA piston to set the final focus of the telescope, one only needs the FSC errors to be sufficiently small to ensure that any one of its actuators are not moving in the wrong direction when commanded within a linear zone, which corresponds to a ~500 step FSC error or larger. Despite the limitations of the SMA hexapod fine stage characterization test due to the global dynamics of the test environment within Chamber A, the test results do show that none of the SMA actuators have gross FSC errors that are large enough to make setting the SMA focus to be a problematic exercise. As such, no corrective action to the SMA hexapod actuators was taken.

6. SUMMARY

In this paper, various methods utilizing several different optical metrology tools (deflectometry, interferometry, and direct imaging) were used to measure and verify the fine stage positional knowledge of the Webb telescope's 132 actuators that are used to position the telescope's optics to nm-levels of precision during deployment, alignment and commissioning, and through the mission lifetime for wavefront control and maintenance. For the 132 actuators, these risk reduction tests identified just six actuators that were sufficiently out of expectation to warrant corrective action. With these corrections, the ensemble distribution of actuator fine stage position uncertainty is sufficient to satisfy the WFS&C requirements for on-orbit alignment and commissioning of the OTE.

ACKNOWLEDGEMENTS

The James Webb Space Telescope project is an international collaboration led by NASA's Goddard Space Flight Center in Greenbelt, MD. Ball Aerospace would like to acknowledge and thank NASA for their leadership, funding, and support during the testing and analysis of the CoC ambient and OTIS cryogenic testing campaigns. The authors would also like to specifically acknowledge the support from the Webb team at Harris, Inc. for collecting and processing the cryogenic fine stage characterization data taken with COCOA. Finally, we would like to thank the many individuals, companies, and government institutions not previously identified who supported the integration and testing effort of the OTIS at both Goddard Space Flight Center and Johnson Space Center.

REFERENCES

[1] Lightsey, P. A., Atkinson, C., Clampin, M., Feinberg, L., "James Webb Space Telescope: Large Deployable Cryogenic Telescope in Space", Optical Engineering, 51, (2012)
[2] Lightsey, P. A. et al. "James Webb Space Telescope optical performance predictions post cryogenic vacuum tests", Proc. SPIE, 10698-3 (2018)
[3] Knight, J. S. et al. "Observatory Alignment of the James Webb Space Telescope", Proc. SPIE, 8442 (2012)
[4] Warden, R. M., "Cryogenic Nano-actuator for JWST", Proceedings of the 38th Aerospace Mechanisms Symposium, Langley Research Center (2006)
[5] Acton, D.S. et al. "Wavefront sensing and controls for the James Webb Space Telescope", Proc. SPIE, 8442 (2012)
[6] Gallagher, B. B. et al. "James Webb Space Telescope mirror and actuator performance at cryo-vacuum", Proc. SPIE, 10698-7 (2018)

[7] Keski-Kuha, R. et al. “JWST OTE center of curvature test”, Proc. SPIE, 10698-125 (2018)
[8] Kimble, R. et al. “James Webb Space Telescope (JWST) optical telescope element and integrated science instrument module (OTIS) cryogenic optical test results”, Proc. SPIE, 10698-4 (2018)
[9] Hadaway, J. B. et al. “Performance of the center-of-curvature optical assembly during cryogenic testing of the James Webb Space Telescope”, Proc. SPIE, 10698-2 (2018)
[10] Coyle, L.E. et al. “Optical assessment of the James Webb Space Telescope primary and secondary mirror cryogenic alignment with a Hartmann test”, Proc. SPIE, 10706-247 (2018)